Kinetic and mechanistic analysis of Mn(II)AA doped hypergolic ignition in HTP/kerosene bipropellant systems

Jindal, Prakhar; Botchu, Jyoti

DOI
10.1016/j.rineng.2025.108699

Publication date
2026

Document Version
Final published version

Published in
Results in Engineering

Citation (APA)
Jindal, P., & Botchu, J. (2026). Kinetic and mechanistic analysis of Mn(II)AA doped hypergolic ignition in HTP/kerosene bipropellant systems. *Results in Engineering*, *29*, Article 108699. https://doi.org/10.1016/j.rineng.2025.108699

Results in Engineering 29 (2026) 108699

Contents lists available at ScienceDirect

Results in Engineering

journal homepage: www.sciencedirect.com/journal/results-in-engineering

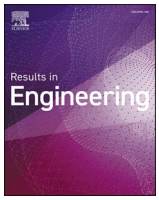

Kinetic and mechanistic analysis of Mn(II)AA doped hypergolic ignition in HTP/kerosene bipropellant systems

Prakhar Jindal *, Jyoti Botchu

Space System Engineering Section, Space Engineering, Faculty of Aerospace Engineering, TU Delft Kluyverweg 1 2629 HS Delft, the Netherlands

ARTICLE INFO

Keywords:
Hypergolic ignition
High-Test Peroxide (HTP)
Manganese (II) acetylacetonate
Ignition delay time (IDT)
Flame temperature
Green bipropellants
Arrhenius kinetics

ABSTRACT

Hypergolic ignition systems have traditionally relied on toxic propellants such as MMH/NTO, prompting a global shift toward greener alternatives. High-Test Peroxide (HTP), with its high oxygen content and clean decomposition products, has emerged as a promising oxidizer when paired with kerosene and suitable catalysts. However, a mechanistic understanding of HTP–fuel ignition, especially with metal-organic catalysts under varying conditions, remains underdeveloped. Here, a comprehensive experimental and kinetic study of hypergolic ignition using Mn (II) acetylacetonate-doped kerosene with HTP is presented across a wide parametric space (HTP: 85–98 %; catalyst: 0.5–10 wt%; O/F: 4.5–7.5; T: 20–50 °C). The results reveal that ignition delay times (IDTs) reduce by over 30 % with preheating and optimal catalyst loading, and deconvoluted phase-wise IDTs show that Mn(II)AA primarily accelerates HTP decomposition and chemical ignition. Derived apparent activation energies ($E_a \approx 10.0$ kJ/mol) are consistently low, while the Arrhenius pre-exponential factor (A) increases significantly with catalyst and oxidizer concentration, indicating catalytic efficiency and diminishing returns beyond 5 wt%. Peak flame temperatures exceeding 1200 °C confirm robust energy release, with high-speed imaging further revealing a transition to rapid, spatially distributed ignition under optimal conditions. These findings offer quantitative mechanistic insights into catalyst-enhanced HTP ignition and establish a framework for optimizing green bipropellant systems for aerospace propulsion.

1. Introduction

Traditional hypergolic propellants, such as monomethylhydrazine (MMH) paired with nitrogen tetroxide (NTO), have long been favored in liquid propulsion systems for their paramount attributes of prompt ignition and reliable storability [1–3]. However, these propellant pairs present severe health and environmental challenges: MMH and related hydrazines are acutely toxic, carcinogenic, and necessitate complex handling procedures to mitigate risks to operators and the environment [4–7]. Occupational exposure limits for hydrazine are exceedingly low, and even minimal contact can result in serious pulmonary, neurological, or organ toxicity [8,9]. These inherent hazards mandate intensive safety protocols around storage facilities and spacecraft fueling operations, significantly escalating operational costs and logistical complexity across the entire mission lifecycle [3–5].

As space agencies and the broader aerospace industry increasingly prioritize greener, safer alternatives, High-Test Peroxide (HTP), highly concentrated hydrogen peroxide (typically 85–98 % by weight), has emerged as a compelling oxidizer option [10–12]. HTP decomposes catalytically or thermally into steam and oxygen, possessing an impressive oxygen mass fraction of approximately 47 %. Its decomposition is highly exothermic, contributing both oxidizer and thermal energy crucial for subsequent fuel ignition [13,14]. Unlike NTO or MMH, HTP is non-carcinogenic and exhibits favorable storage characteristics at ambient temperature, rendering it an attractive candidate for clean and sustainable propulsion [7,12,15]. Historically, pioneering systems, such as the British "Gamma" engine, successfully utilized HTP with kerosene and catalyst assemblies to achieve efficient and repeatable hypergolic ignition, demonstrating its early utility [16,17].

The catalytic ignition in HTP-based propellant systems is a multi-step process initiated by the rapid decomposition of HTP upon contact with a suitable catalyst. This decomposition is highly exothermic and proceeds via a complex radical chain mechanism, which the catalyst significantly facilitates by lowering the activation energy and generating highly reactive intermediate species [18]. The overall stoichiometric decomposition reaction of HTP is:

* Corresponding author.
E-mail address: p.jindal@tudelft.nl (P. Jindal).

https://doi.org/10.1016/j.rineng.2025.108699
Received 1 September 2025; Received in revised form 2 December 2025; Accepted 10 December 2025
Available online 11 December 2025

$$2H_2O_2 \xrightarrow{catalyst} 2H_2O(g) + O_2(g) + Heat \quad (1)$$

The detailed catalytic mechanism, particularly involving transition metal ions (M), typically involves the formation and propagation of hydroxyl (HO·) and hydroperoxyl (HO_2·) radicals:

Initiation:

$$\begin{aligned} H_2O_2 + M^{n+} &\rightarrow HO\cdot + M^{(n+1)+} + OH^- \\ H_2O_2 + M^{(n+1)+} &\rightarrow HO_2\cdot + M^{n+} + H^+ \end{aligned} \quad (2)$$

Propagation:

$$\begin{aligned} H_2O_2 + HO\cdot &\rightarrow HO_2\cdot + H_2O \\ HO_2\cdot + HO\cdot &\rightarrow H_2O + O_2 \end{aligned} \quad (3)$$

(Other radical-radical reactions also occur, leading to chain branching or termination)

Upon the HTP contacting the catalyzed fuel mixture, the catalyst immediately initiates these radical reactions. This rapid decomposition generates a significant amount of heat and gaseous oxygen directly within the fuel pool. The synergistic combination of this high local temperature and the presence of these nascent, highly reactive oxygen species (including O_2 and the radicals like HO· and HO_2·) then causes the hydrocarbon fuel to spontaneously ignite [19]. This process ensures the prompt and reliable ignition characteristic of hypergolic propellants.

Critical to HTP's broader utility in modern propulsion is ensuring consistently rapid and reliable ignition performance. Uncatalyzed HTP-kerosene systems typically exhibit long and inconsistent ignition delays, which can lead to unreliable combustion or dangerous hard starts, a major concern during transient thruster operations [20,21]. Earlier work has demonstrated that the incorporation of specific metal-organic catalysts, particularly Fe (III), Co (II), Mn (II)/(III), MnO_x and Cu (II), can significantly reduce ignition delay times (IDTs) to under 10 ms in peroxide pressurized environments [11,22–25]. While manganese acetylacetonate (Mn(II)AA) has shown efficacy in catalyzing peroxide-fuel ignition in other liquid fuels, such as ethanol, demonstrating sub-10 ms ignition delays in those contexts [25–28], the performance of Mn (II)AA when blended with kerosene and combined with HTP across a comprehensive operational envelope has not yet been thoroughly investigated.

This research, therefore, aims to fill this critical knowledge gap by conducting an exhaustive experimental campaign and providing a comprehensive dataset. The study evaluates Mn(II)AA-doped kerosene with HTP across a broad range of operating conditions: varying catalyst loadings (0.5–10 % by weight), oxidizer concentrations (85–98 %), stoichiometric ratios (O/F 4.5–7.5), and temperature conditions (20 °C ambient and 50 °C preheated fuel). Ignition delay times (IDTs) were systematically assessed using repeatable open-air drop tests. Beyond macroscopic IDT measurements, this study uniquely contributes by: (1) Quantitatively mapping critical thermal regimes including HTP decomposition onset, fuel preheat, kerosene autoignition, and chemical ignition, thereby decomposing the overall IDT into its distinct mechanistic phases. (2) Deriving fundamental Arrhenius kinetic parameters (activation energy and pre-exponential factor A) across various HTP purities and catalyst loadings. (3) Quantifying the catalytic efficiency by identifying optimal catalyst loadings and rigorously delineating the point of diminishing returns based on kinetic insights. And (4) Correlating these findings with post-ignition peak flame temperatures to provide a holistic understanding of the system's performance and energy release. This research offers novel, multi-faceted insights crucial for the rational design and optimization of sustainable, high-performance propulsion systems utilizing HTP and catalytic fuels.

2. Materials and methods

2.1. Propellants and catalyst preparation

Commercial kerosene ($C_{15}H_{32}$, lab grade, CAS No. 8008-20-6) was used as the fuel, supplied by Chemwatch. It was used without any prior filtration or drying. Hydrogen Peroxide (HTP) was initially obtained as a 70 % (w/w) technical grade solution from Chemwatch (CAS No. 7722-84-1). Higher concentrations of HTP, up to 98 % (w/w), were subsequently prepared using a gas-phase dehydration method, using a patented technology described in Patents US17775065 [29] and NL2024229B1 [30]. Specific HTP concentrations (85 %, 87 %, 90 %, 93 %, and 95 % w/w) for the experiments were prepared by diluting the 98 % (w/w) stock with deionized water. To ensure strict chemical stability and consistency, concentrations were verified using a calibrated digital refractometer immediately before the experimental campaign and re-verified weekly during storage. A strict acceptance window of ±0.25 % (w/w) was enforced; any solution showing a deviation greater than this limit was discarded and prepared fresh. All HTP solutions were stored in vented high-density polyethylene capped borosilicate glass containers within a refrigerator maintained at 2 °C in a dark environment to ensure stability.

Manganese (II) acetylacetonate (Mn(II)AA, Mn $(C_5H_7O_2)_2$, 99 % pure, CAS No. 14024-58-9) was purchased from Chemwatch. The catalyzed kerosene mixtures were prepared by precisely weighing the Mn(II)AA using a precision weighing scale available in the Chemistry laboratory at Aerospace Engineering, Delft University of Technology. The weighed Mn(II)AA was then dissolved directly into the kerosene by vigorous magnetic stirring for 26–32 h at 30 °C until a visually homogeneous solution was obtained. No other solvents were used in the preparation. Catalyst loadings, ranging from 0.5 % to 10 % (w/w) of Mn(II)AA in kerosene, were precisely achieved by direct mass measurement.

2.2. Experimental setup: open-air drop test apparatus

Ignition delay time (IDT) measurements were conducted in an open-air environment at ambient pressure using the experimental setup schematically presented in Fig. 1. The experiments were conducted within a 2 mL borosilicate glass bottle as the reaction chamber, positioned inside a fume hood for safety. The experimental setup involved a precision syringe pump (NE-1000, New Era Pump Systems Inc.) used for dispensing HTP. The doped kerosene was first carefully poured into the 2 mL glass bottle, forming a quiescent pool.

For each test, a fixed volume of 0.27 mL (270 μL) of HTP was sprayed onto the doped kerosene pool using an 18-gauge stainless steel dispensing blunt needle, which had a 1.2 mm outer diameter and a length of 1.96 inches (49.9 mm). The pump flow rate was set to 20 mL/min to generate a consistent continuous liquid jet (Rayleigh breakup) rather than a dispersed spray, ensuring reproducible impact momentum. A fixed needle-to-pool standoff distance of 120 mm was maintained to prevent splash-back while ensuring effective impingement. The volume of the catalyzed kerosene kept in the glass bottle was varied to achieve the desired oxidizer-to-fuel (O/F) mass ratios: 0.102 mL for O/F 4.5, 0.084 mL for O/F 5.5, 0.071 mL for O/F 6.5, and 0.061 mL for O/F 7.5. The delivered O/F mass ratios were calculated based on the precise volumetric displacement of the syringe pump and the fluid densities, assuming negligible evaporation losses during the rapid dispensing phase (<1 s). The oxidizer jet impinged vertically onto the static kerosene pool, initiating the reaction.

Experiments were conducted at two temperatures: ambient (20 °C) and preheated (50 °C). Preheating was achieved using a laboratory hot plate, with the bottle temperature monitored using a contact-type digital thermometer. Post-ignition flame temperatures were acquired using a FLIR A655sc infrared camera (spectral range 7.5–14.0 μm, resolution 640 × 480) equipped with a standard 25° lens. The camera operated under valid factory radiometric calibration. Radiometric data processing was performed in FLIR Research Studio. A constant emissivity (∈) of 0.96 was applied, consistent with literature values for optically thick, soot-laden hydrocarbon diffusion flames. To quantify measurement confidence, a sensitivity analysis was performed considering an emissivity range of 0.88 to 0.98, resulting in a reported uncertainty of ±20 °C

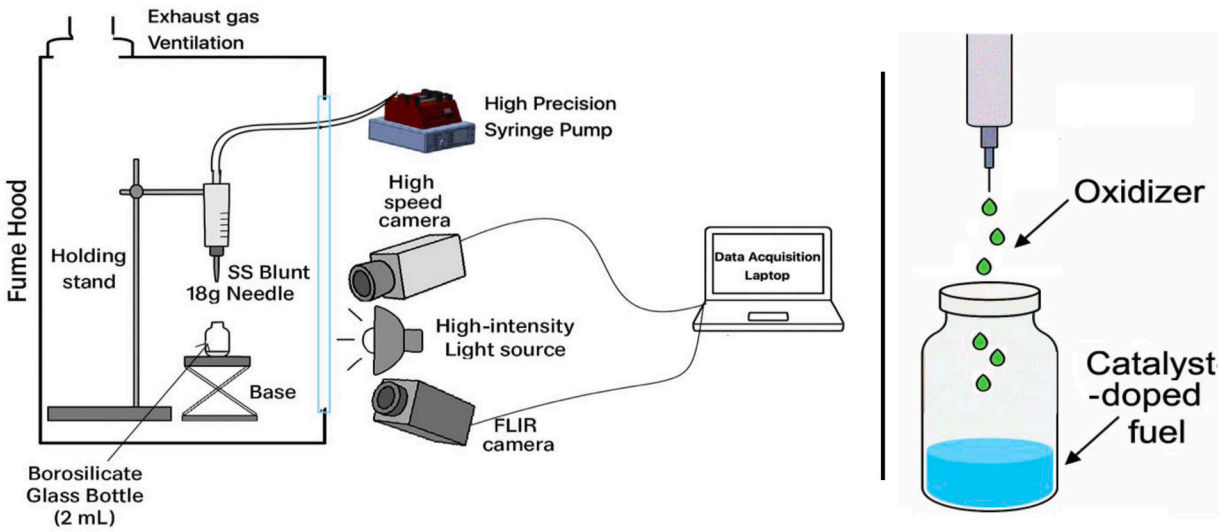

Fig. 1. Schematic illustration of the open-air drop test apparatus and the propellant dispensing method. The setup (left) includes a precision syringe pump with an 18 G needle for oxidizer dispensing into a 2 mL borosilicate glass bottle, all housed within a fume hood, with high-speed and FLIR cameras for data acquisition. The right panel depicts the oxidizer droplets impacting the catalyst-doped fuel pool.

for the peak temperatures. The reflected apparent temperature was set to ambient (20 °C). Spatial sampling focused on the dynamic maximum temperature within a defined Region of Interest (ROI) centered on the flame kernel, ensuring that the reported values reflect the core combustion intensity rather than cooler plume edges.

2.3. Ignition delay time (IDT) measurement and phase deconvolution

The ignition delay time (IDT) was defined as the duration between the first physical contact of the oxidizer droplet with the catalyzed fuel and the onset of observable light emission (spark or flame). A Photron FASTCAM NOVA S6 high-speed camera (CMOS, 1024 × 1024 resolution) operating at 6400 fps was used to record the events. Illumination was provided by a high-lumen (17,672 lm), 5600 K white light source, focused on the reaction zone to ensure visibility of initial decomposition and ignition phases.

A novel methodology was employed to deconvolve the overall IDT into its distinct mechanistic phases, derived from frame-by-frame analysis of the high-speed videos. To ensure objectivity and minimize measurement drift, specific visual thresholds were applied:

- *HTP Decomposition IDT (IDT_{dec}):* Time from droplet contact to the first frame showing continuous gas evolution (fume release) distinct from the initial droplet impact splash.
- *Physical IDT (IDT_{phy}):* Time from the end of decomposition to the formation of an expanding vapor cloud indicative of active vaporization.
- *Chemical IDT (IDT_{chem}):* Time from vapor cloud formation to 'First Light', defined as the first frame where local pixel intensity exceeded a threshold of 20 % above the background baseline, signaling the onset of chemiluminescence.

The visual 'First Light' timestamps were further validated against thermal data from the FLIR camera, where a sharp inflection in the temperature profile consistently corroborated the onset of the chemical ignition phase. The video data were analyzed using PFV software (Photron) for the high-speed camera, and thermal imaging data were processed using FLIR Research Studio.

The total IDT was expressed as:

$$IDT = DecompositionDelay + PhysicalIDT + ChemicalIDT$$

Kinetic Analysis: Activation Energy and Arrhenius Factor Derivation

The temperature dependence of the ignition delay time was assumed to follow the Arrhenius equation, enabling the determination of apparent activation energy (E_a) and apparent Arrhenius pre-exponential factor (A). A two-point Arrhenius calculation method was applied for each catalyst weight percentage. IDTs were precisely measured at two distinct temperatures (20 °C and 50 °C) for a selected subset of conditions to facilitate this analysis: HTP concentrations of 95 % and 98 %; O/F ratios of 7.5 and 6.5; and catalyst loadings of 2.5 %, 3 %, 3.5 %, 4 %, 4.5 %, 5 %, 7.5 %, and 10 %.

The activation energy (E_a) was calculated using the following formula:

$$\boldsymbol{E_a} = \frac{\boldsymbol{R}(\ln(\boldsymbol{IDT}_2) - \ln(\boldsymbol{IDT}_1)}{(1/\boldsymbol{T}_1 - 1/\boldsymbol{T}_2)} \tag{4}$$

where R is the universal gas constant (8.314 J/mol·K), T_1 and T_2 are the absolute temperatures in Kelvin (293.15 K and 323.15 K, respectively), and IDT_1 and IDT_2 are the ignition delay times measured at T_1 and T_2, respectively.

The Arrhenius pre-exponential factor (A) was then calculated using the formula (with IDT in seconds):

$$\boldsymbol{A} = \boldsymbol{e}^{\left(-\frac{E_a}{RT_1}\right)} \cdot \frac{1}{\boldsymbol{IDT}_1} \tag{5}$$

2.4. Experimental matrix and data reliability

A comprehensive experimental matrix was investigated, encompassing HTP concentrations from 85 % to 98 % (w/w), Mn(II)AA catalyst loadings from 0.5 % to 10 % (w/w), oxidizer-to-fuel (O/F) mass ratios of 4.5, 5.5, 6.5, and 7.5, and initial temperatures of 20 °C and 50 °C, all at ambient pressure. For each experimental condition, a minimum of 5 replicate tests were performed to ensure data reliability and reproducibility. Results are presented as mean values. No specific outlier criteria were applied to exclude data points from the analysis; all measured data points were considered.

2.5. Statistical analysis

For every experimental condition defined by HTP concentration, catalyst loading, and O/F ratio, a minimum of five independent replicates ($n = 5$) were conducted to ensure data reliability. Results in the

following sections are reported as the mean ± standard deviation (SD) to quantify the dispersion and repeatability of the ignition events. No outlier rejection criteria were applied; all captured data points were included in the statistical analysis to present a transparent view of ignition consistency.

3. Results and discussion

This section presents the experimental findings on the hypergolic ignition characteristics of Mn(II)AA-doped kerosene with HTP. The discussion is integrated with the results, providing immediate interpretation and mechanistic insights into the observed phenomena. The experiments covered variations in HTP concentration (85 %, 87 %, 90 %, 93 %, 95 %, 98 %), Mn(II)AA catalyst weight percentage (0.5 %, 1 %, 1.5 %, 2 %, 2.5 %, 3 %, 3.5 %, 4 %, 4.5 %, 5 %, 7.5 %, 10 %), oxidizer-to-fuel ratios (O/F of 4.5, 5.5, 6.5, and 7.5), and two initial fuel mixture temperatures (20 °C and 50 °C).

3.1. Ignition characteristics across composition space

A comprehensive experimental campaign was conducted to investigate ignition characteristics across an extensive parametric space systematically. A total of 576 unique drop test conditions were performed, each replicated at least five times ($n = 5$) to ensure data consistency and reliability. The data presented in Figs. 3, 4, 8 and 10 include error bars representing the standard deviation derived from these replicates. The observed variance was generally low (standard deviation typically <10 % of the mean IDT), indicating the high repeatability of the drop test method. The complete dataset of ignition delay times (IDTs) is provided as Supplementary Table S1.

Fig. 2 summarizes the entire dataset in a concise, color-coded ignition outcome matrix. In this figure, each cell represents the ignition behavior observed under specific experimental conditions, color-coded for easy interpretation: green indicates consistent ignition in all test replicates, yellow represents partial or inconsistent ignition, and red denotes no ignition across all replicates. Critically, Fig. 2 distinctly separates the ignition outcomes obtained at two initial fuel mixture temperatures (20 °C and 50 °C), providing a clear comparison of temperature effects on ignition reliability across the investigated parameter space.

Analyzing Fig. 2 reveals important trends in ignition behavior and clearly highlights the operational thresholds required to achieve reliable hypergolic ignition. At the ambient initial temperature (20 °C), Fig. 2(a), catalyst loadings below approximately 2.5 wt % and HTP concentrations of 90 % or below frequently resulted in either partial or no ignition, particularly at lower O/F ratios (4.5 and 5.5). Increasing catalyst loading above 2.5 wt % and employing higher HTP concentrations (≥93 %) significantly improved ignition consistency, especially at elevated O/F ratios (≥6.5). At these conditions, the system transitions into a robust ignition regime (green area), demonstrating reliable ignition across all replicates.

The impact of elevated initial fuel mixture temperature (50 °C) is notably distinct. As evident in Fig. 2(b), increasing the initial temperature to 50 °C significantly expands the reliable ignition envelope (green zone), even at relatively lower catalyst loadings and HTP concentrations. Conditions at 50 °C, which previously showed partial ignition or borderline results at 20 °C, reliably transitioned to consistent ignition. This demonstrates the beneficial impact of elevated initial temperature, which likely enhances reaction kinetics through improved decomposition rates of HTP and enhanced volatility of kerosene, thereby promoting rapid ignition even at relatively marginal conditions.

To quantitatively understand these trends further, Fig. 3 provides plots of measured IDTs versus catalyst weight percentage across all O/F ratios and HTP concentrations at an ambient initial temperature of 20 °C. These plots further highlight the role of catalyst loading, oxidizer concentration, and O/F ratio in governing ignition delays. Increasing catalyst concentration consistently reduces IDTs, most notably up to approximately 5 wt %, beyond which further catalyst addition yields diminishing returns. For instance, at O/F of 7.5 and 98 % HTP, IDT decreases from approximately 89 ms at 2.5 wt % catalyst to around 67 ms at 5 wt %, with negligible additional improvement (~59 ms) observed at 10 wt %.

Higher HTP concentrations also significantly shorten ignition delays, underscoring the importance of oxidizer quality. For example, at an O/F of 6.5 with 3 wt % catalyst, increasing HTP concentration from 85 % to 98 % reduced IDT from approximately 131 ms to 96 ms. Similarly, higher O/F ratios (6.5 and 7.5) resulted in shorter delays and more consistent ignition compared to lower O/F ratios (4.5 and 5.5), confirming the benefits of slight oxidizer-rich mixtures in achieving rapid ignition. Higher O/F likely enhances the availability of oxygen radicals

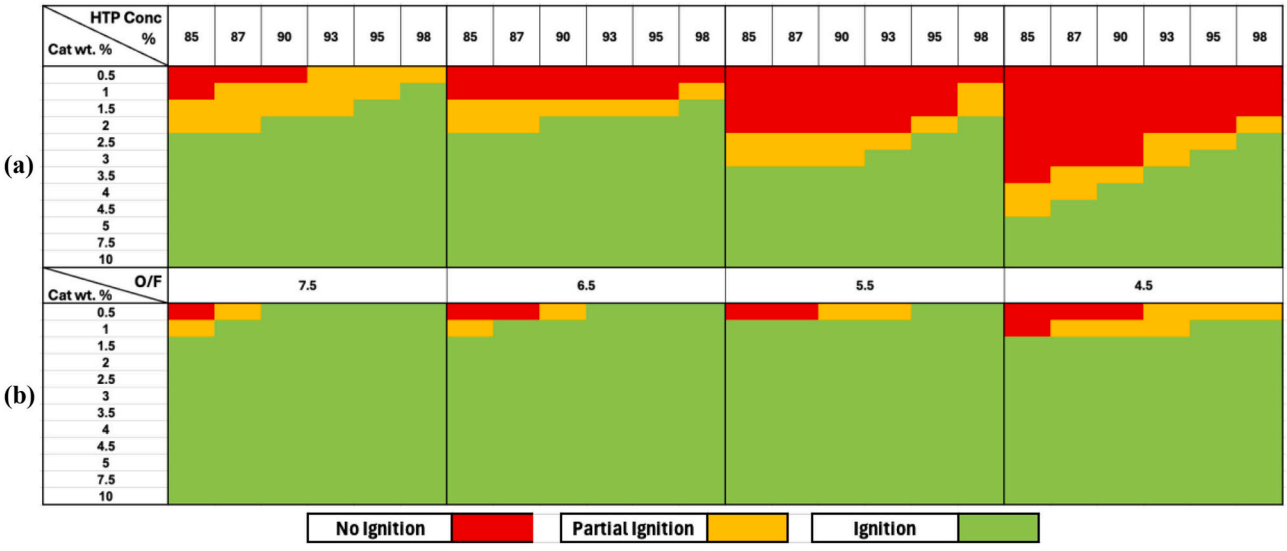

Fig. 2. Ignition reliability map depicting the hypergolic ignition outcomes under various experimental conditions. The matrix shows results for varying HTP concentrations (85 % to 98 %), catalyst weight percentages (0.5 % to 10 %), and oxidizer-to-fuel (O/F) ratios (7.5, 6.5, 5.5, 4.5). Panel (a) represents tests conducted at 20 °C initial temperature, while Panel (b) shows results at 50 °C initial temperature. Green indicates consistent ignition, yellow indicates partial or inconsistent ignition, and red denotes no ignition across all replicates.

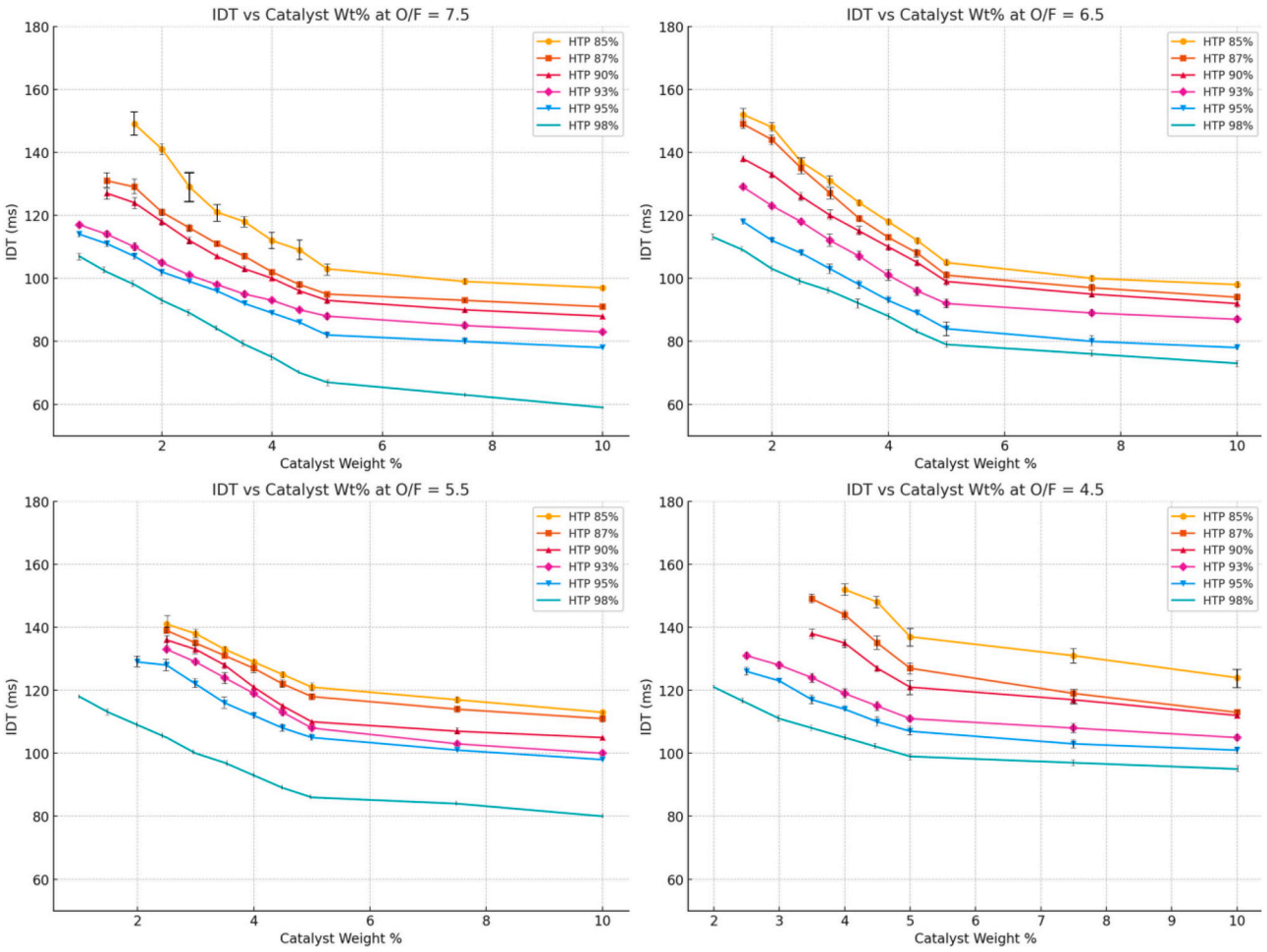

Fig. 3. Measured Ignition Delay Times (IDT) as a function of catalyst weight percentage for various HTP concentrations and Oxidizer-to-Fuel (O/F) ratios at an ambient initial temperature of 20 °C. The plots illustrate the impact of catalyst loading, HTP concentration, and O/F ratio on ignition delay, consistently showing a reduction in IDT with increased catalyst loading and HTP concentration, alongside exhibiting diminishing returns with increased catalyst concentration beyond approximately 5 wt %. Error bars represent the standard deviation ($n = 5$). In many instances, the error bars are smaller than the data symbols due to the high repeatability of the measurements.

during decomposition, accelerating ignition onset.

The detailed ignition characterization presented here clearly defines an operational envelope for reliable ignition of Mn(II)AA-catalyzed HTP–kerosene propellant mixtures under ambient pressure conditions. Reliable ignition occurs most consistently within the following conditions: catalyst loading of 2.5 wt % or higher, HTP concentration of 93 % or higher, and O/F ratios of 6.5 or higher. Furthermore, elevated initial fuel temperature (50 °C) significantly widens the ignition envelope and reduces IDTs compared to ambient (20 °C). Outside this identified parameter range, ignition reliability sharply diminishes, reinforcing the necessity for controlled optimization in practical propulsion applications.

3.2. *Initial mixture temperature effects on ignition delay*

The initial temperature of the propellant mixture strongly influences the catalytic ignition process, significantly affecting both ignition reliability and delay times. As highlighted in Section 3.1, an increase in initial temperature from 20 °C to 50 °C distinctly expanded the "Ignition" regions across the entire operational matrix (Fig. 2), signaling enhanced robustness. This beneficial impact is not only observed in reduced ignition delay times but also in the marked improvement of overall ignition outcomes.

Specifically, a closer examination of Table S1 reveals that many cases exhibiting "No ignition" at 20 °C successfully transitioned to complete ignition at 50 °C. For instance, at O/F 6.5, 93 % HTP, and 0.5 % catalyst, no ignition was recorded at 20 °C, but reliable ignition occurred at 50 °C with an IDT of 93 ms. Similarly, conditions that showed "Partial ignition" at 20 °C were frequently converted to consistent, complete ignition at 50 °C. This demonstrates that elevated temperature overcomes critical thresholds, enabling the system to reliably ignite under conditions that were previously challenging or unviable. The enhanced initial thermal energy effectively broadens the operational window for hypergolic ignition.

Beyond this improved reliability, a consistent and substantial reduction in IDT was observed for nearly all conditions where ignition was achieved at both temperatures. For instance, at an O/F ratio of 7.5 with 95 % HTP, increasing the catalyst loading from 2.5 % to 5 % reduced the IDT from 99 ms to 82 ms at 20 °C. Under identical conditions, at 50 °C, the IDTs for the same catalyst loadings decreased from 67 ms to 55 ms. This represents an approximate 32 % reduction in IDT (e.g., for 2.5 % catalyst, $(99-67)/99 \times 100\ \% \approx 32.3\ \%$) across this range. Even more noticeably, for the most favorable conditions (98 % HTP, 10 % catalyst, O/F 7.5), the IDT decreased from 59 ms at 20 °C to 40 ms at 50 °C, a reduction of approximately 32.2 %. Similar trends were observed across other O/F ratios and HTP concentrations where ignition was achieved. For instance, at O/F 5.5 with 98 % HTP and 5 % catalyst, the IDT decreased from 86 ms at 20 °C to 58 ms at 50 °C, representing a

32.5 % reduction.

To further quantify this widespread improvement, Fig. 4 presents the average percentage reduction in IDTs across the various O/F ratios when the initial temperature is increased from 20 °C to 50 °C. This calculation is strictly based on a paired sensitivity analysis, including only those experimental conditions where reliable ignition was achieved at both 20 °C and 50 °C (Sample size $N \approx$ 20–40 unique conditions per O/F). Cases resulting in 'No Ignition' or 'Partial Ignition' at 20 °C were excluded to avoid skewing the metric with arbitrary values. Consequently, the reported 32–33 % reduction represents a conservative baseline; the practical benefit is likely higher for marginal mixtures where preheating transitions the system from non-ignition to robust combustion.

As Fig. 4 illustrates, the average percentage reduction consistently falls within a narrow range of approximately 32.46 % to 33.43 %. The error bars included in the figure represent the standard deviation of these reduction percentages across the varying catalyst loadings and HTP concentrations within each O/F category. The narrow dispersion indicated by these bars demonstrates that the accelerating effect of preheating is systematic and robust, occurring uniformly across the diverse parametric space rather than being driven by isolated outliers. This remarkable consistency across diverse O/F ratios highlights the uniform beneficial impact of elevated initial temperature as a control parameter for achieving rapid ignition. This substantial IDT reduction at elevated temperatures directly results from faster chemical kinetics. According to the Arrhenius principle, reaction rates increase exponentially with temperature, meaning that increasing the initial thermal energy of the system provides molecules with more energy to overcome activation barriers. Specifically, a higher initial temperature facilitates more rapid decomposition of HTP by the Mn(II)AA catalyst, leading to a quicker generation of highly reactive oxygen species and heat. Additionally, the elevated temperature enhances the volatility of kerosene, accelerating its vaporization and mixing with the gaseous products from HTP decomposition. The combined effects of faster HTP decomposition, quicker fuel vaporization, and an overall increase in molecular collision frequency jointly contribute to a significantly shortened pre-ignition phase and thus reduced IDT.

Furthermore, high-speed camera images captured during the experiments provided visual evidence of the ignition event and subsequent flame development. These images revealed that increasing the initial temperature from 20 °C to 50 °C generally correlated with a more rapid and stable transition from decomposition to full flame. For instance, visual sequences for conditions such as O/F 6.5, 93 % HTP, and 2.5 % catalyst clearly showed a more immediate and spatially uniform flame propagation at 50 °C compared to 20 °C, where initial flame kernels might have been less robust or slower to develop. These visual assessments of flame robustness, vigor, and uniformity were qualitative, based on observed immediacy, spatial distribution, and stability during propagation, rather than quantifiable metrics like specific brightness levels or calculated area growth. This qualitative observation from high-speed imaging complements the quantitative IDT data, confirming that elevated initial temperatures foster a more vigorous initial energy release and efficient combustion.

Fig. 5 provides a comprehensive visual insight into the hypergolic ignition progression, highlighting the distinct effects of initial temperature and catalyst weight percentage. Fig. 5(a) shows the ignition sequence for HTP 95 % with 2.5 wt % catalyst, while Fig. 5(b) presents the same for HTP 95 % with 4.5 wt % catalyst, both compared at 20 °C (top row) and 50 °C (bottom row) initial temperatures. Each sequence captures five critical stages of the ignition event, from initial contact to flame stabilization, with precise timestamps enabling direct comparison.

The detailed visual observations and comparative analysis for each time step are summarized in Table 1, quantifying how initial temperature and catalyst loading influence the speed of each stage of the ignition process. A clear accelerating effect of elevated temperature is consistently observed from the earliest stages, with visible pre-ignition activity and "first light" occurring significantly faster at 50 °C compared to 20 °C. For instance, at the timestamps where 50 °C conditions achieve ignition (e.g., 60 ms for 4.5 wt % catalyst), the corresponding 20 °C conditions consistently show no visible flame, igniting only much later. Beyond temperature, increasing catalyst loading from 2.5 wt % to 4.5 wt % also consistently shortens IDTs and accelerates flame development at both temperatures, demonstrating its synergistic effect on ignition kinetics.

Under optimal conditions, particularly at 50 °C with 4.5 wt % catalyst (Fig. 5(b), bottom row), the ignition process is notably rapid and vigorous. In these instances, the typical propagation from a distinct localized kernel is largely bypassed; instead, the combustion appears as a near-instantaneous burning of the vapor plume (e.g., Fig. 5(b), 50 °C at 60 ms). This observation is indicative of rapid, spatially distributed ignition (ignition that occurs uniformly throughout the vapor phase with negligible flame front propagation time), signifying extremely short

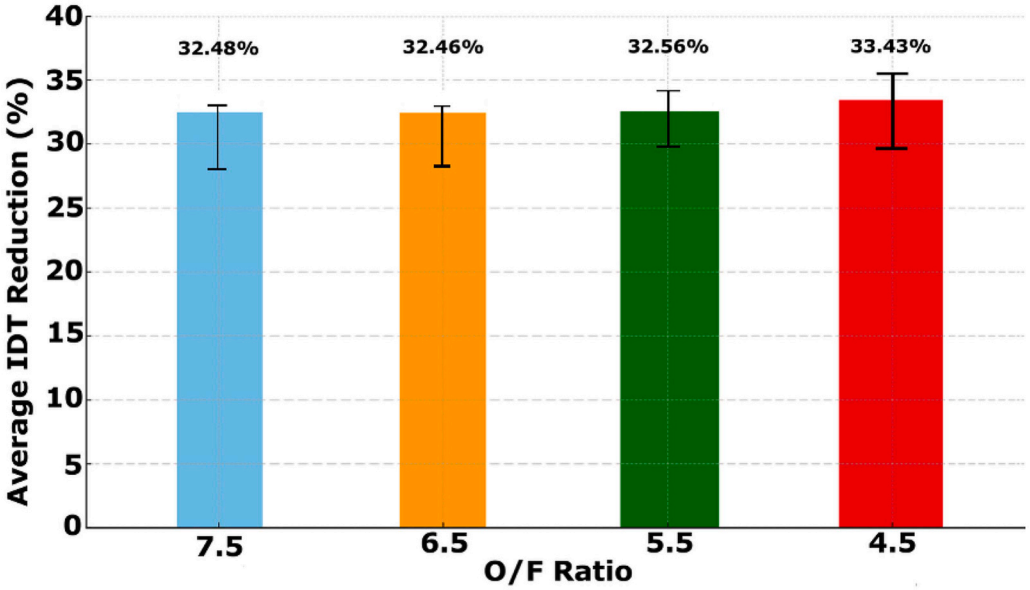

Fig. 4. Average percentage reduction in ignition delay time when initial fuel mixture temperature is increased from 20 °C to 50 °C, categorized by O/F ratio. Data represents only paired conditions where ignition was successful at both temperatures ($N \approx$ 20–40 unique conditions per bar). Error bars represent the standard deviation.

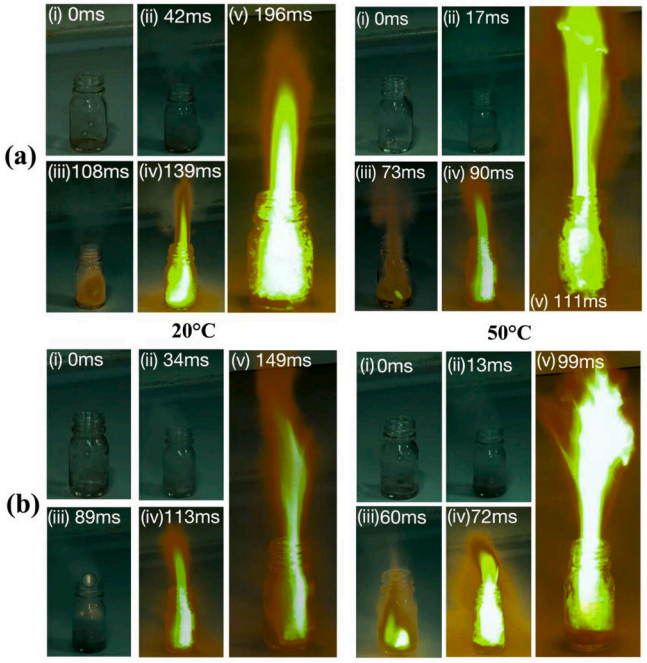

Fig. 5. High-speed camera image sequences illustrating the combined effects of initial temperature and catalyst weight percentage on hypergolic ignition and flame development. The figure presents conditions at HTP 95 % and O/F 6.5 for (a) 2.5 wt % Mn(II)AA catalyst and (b) 4.5 wt % Mn(II)AA catalyst. Each panel shows comparative sequences for 20 °C (Left up and down) and 50 °C Right up and down) initial temperatures, capturing five critical stages: (i) initial propellant contact, (ii) onset of reaction, (iii) first light, (iv) early flame development, and (v) flame stabilization. Timestamps on each frame quantify the significant acceleration of ignition and flame establishment with increasing temperature and catalyst loading.

physical and chemical delays where the critical conditions for chemical reaction are met almost simultaneously across a significant volume of the vapor phase.

The observed flames in all conditions are predominantly luminous yellow-orange diffusion flames, characteristic of kerosene combustion. At 50 °C, the flames establish with greater vigor, luminosity, and achieve a more stable, columnar shape at earlier stages compared to 20 °C. This suggests that the higher initial temperature leads to more intense and efficient combustion in the initial moments, likely due to enhanced reaction rates and improved vaporization rates. Consequently, incorporating preheating strategies or warm-start conditions could significantly reduce igniter requirements and improve ignition reliability for propulsion systems utilizing similar hypergolic blends. Furthermore, higher catalyst loading also contributes to a slightly more vigorous initial flame development, consistent with its effect on reducing IDT. Overall, Fig. 5 provides compelling visual evidence that elevating initial temperature and optimizing catalyst concentration synergistically contribute to significantly reducing ignition delays and fostering more robust and efficient hypergolic ignition.

3.3. Time-resolved ignition dynamics and deconvolution

Understanding the intricate steps of hypergolic ignition extends beyond merely measuring a total ignition delay time (IDT). A deeper mechanistic insight can be gained by deconvoluting the overall IDT into distinct phases, each governed by different underlying phenomena: hydrogen peroxide (HTP) decomposition, physical mixing (vaporization and diffusion), and the final chemical reaction leading to rapid heat release and ignition. Furthermore, identifying the characteristic temperatures attained at critical junctures within these phases provides valuable thermodynamic context. For these measurements, the case with elevated initial mixture temperature (50 °C) was considered, as this case yielded more promising IDT values compared to ambient temperatures. This section presents both the time contributions of each phase (ms) and their associated characteristic temperatures (°C) to explain the rate-limiting steps and the precise roles of various operational parameters.

3.3.1. Phase-wise ignition delay times (ms)

The overall ignition delay time (IDT) was deconvoluted into three distinct temporal phases: HTP decomposition IDT, Physical IDT, and Chemical IDT. These values, along with the total IDT, are presented in Table 2 for various O/F ratios, HTP concentrations, and catalyst loadings. To visually represent the contributions of each phase to the total IDT, Fig. 6 provides stacked bar charts. Detailed data, including the standard deviation for each specific phase, is provided in Table 2.

Analysis of Table 2 and Fig. 6 reveals distinct trends in how each phase contributes to the overall ignition delay. Increasing the catalyst weight percentage consistently reduces the duration of all three phases, leading to a shorter overall IDT. However, the HTP Decomposition IDT and Chemical IDT phases exhibit the most pronounced reductions. For instance, at O/F 7.5 with 98 % HTP, increasing catalyst from 2.5 % to 5.0 % reduced HTP Decomposition IDT from 14 ms to 9 ms, and Chemical IDT from 25 ms to 20 ms. In contrast, the Physical IDT remains relatively stable. Crucially, the relatively small standard deviation observed in the Physical IDT phase (evident in Table 2) across varying catalyst loadings statistically validates the conclusion that this phase is less sensitive to catalytic boosting than the chemical reaction steps. This indicates that while the catalyst accelerates all active steps, its primary impact is on accelerating the chemical reactions and the initial HTP decomposition, which in turn facilitates faster overall ignition.

Higher HTP concentrations generally result in shorter IDTs across all catalyst loadings. This improvement is largely driven by reductions in the HTP Decomposition IDT and Chemical IDT phases. For example, at O/F 7.5 with 5.0 % catalyst, increasing HTP concentration from 93 % to

Table 1
Comparative visual progression of hypergolic ignition from high-speed camera footage (HTP 95 %, O/F 6.5).

Stage	Description	2.5 wt % Cat (Timestamp from Fig. 5a)			4.5 wt % Cat (Timestamp from Fig. 5b)			Key Comparative Observation
		@ 20 °C	@ 50 °C	ΔT	@ 20 °C	@ 50 °C	ΔT	
(i)	Initial Propellant Contact	0 ms	0 ms	**0 ms**	0 ms	0 ms	**0 ms**	All conditions appear identical at initial contact, with no visible reaction.
(ii)	Onset of Reaction (Fume/Gas Evolution)	42 ms	17 ms	**25 ms**	34 ms	13 ms	**21 ms**	Elevated temperatures and higher catalyst loadings significantly accelerate the onset of visible pre-ignition activity (fume evolution/liquid agitation).
(iii)	First Light (Chemical Ignition)	108 ms	73 ms	**35 ms**	89 ms	60 ms	**29 ms**	First light occurs substantially earlier at 50 °C and with higher catalyst weight; at the 50 °C ignition timestamps, 20 °C conditions show no visible flame.
(iv)	Early Flame Development	139 ms	90 ms	**49 ms**	113 ms	72 ms	**41 ms**	Flame growth is more rapid and appears more vigorous at higher temperatures and catalyst loadings following first light.
(v)	Flame Stabilization	196 ms	111 ms	**85 ms**	149 ms	99 ms	**50 ms**	Full flame stabilization is achieved significantly faster at higher temperatures and catalyst loadings, indicating a more robust combustion process.

Table 2
Deconvoluted ignition delay times (ms) for various conditions.

O/F Ratio	HTP Conc (%)	Catalyst Wt.%	HTP Decomposition IDT (ms)	Physical IDT (ms)	Chemical IDT (ms)	Total IDT (ms)
7.5	93	2.5	16 ± 2	22 ± 1	30 ± 2	68 ± 3
		3.0	15 ± 1	21 ± 2	30 ± 2	66 ± 2
		3.5	14 ± 2	20 ± 1	30 ± 3	64 ± 2
		4.0	13 ± 3	19 ± 2	31 ± 1	63 ± 2
		4.5	12 ± 1	18 ± 2	31 ± 2	61 ± 3
		5.0	11 ± 2	17 ± 3	31 ± 1	59 ± 2
	95	2.5	17 ± 2	23 ± 2	27 ± 1	67 ± 3
		3.0	16 ± 1	22 ± 1	27 ± 2	65 ± 2
		3.5	15 ± 3	21 ± 2	26 ± 2	62 ± 1
		4.0	14 ± 2	20 ± 1	26 ± 3	60 ± 2
		4.5	13 ± 1	19 ± 2	26 ± 1	58 ± 3
		5.0	12 ± 2	18 ± 2	25 ± 2	55 ± 1
	98	2.5	14 ± 2	21 ± 3	25 ± 1	60 ± 2
		3.0	13 ± 1	20 ± 2	24 ± 2	57 ± 3
		3.5	12 ± 3	19 ± 1	22 ± 3	53 ± 2
		4.0	11 ± 2	18 ± 2	22 ± 1	51 ± 2
		4.5	10 ± 1	17 ± 1	20 ± 2	47 ± 3
		5.0	9 ± 2	16 ± 3	20 ± 1	45 ± 2
6.5	93	2.5	18 ± 2	26 ± 3	36 ± 1	80 ± 2
		3.0	17 ± 1	24 ± 2	35 ± 2	76 ± 3
		3.5	16 ± 3	22 ± 1	34 ± 1	72 ± 2
		4.0	15 ± 2	20 ± 2	33 ± 3	68 ± 1
		4.5	14 ± 1	18 ± 3	33 ± 2	65 ± 2
		5.0	13 ± 2	17 ± 1	32 ± 2	62 ± 3
	95	2.5	17 ± 3	25 ± 2	31 ± 1	73 ± 2
		3.0	16 ± 1	23 ± 1	31 ± 3	70 ± 2
		3.5	15 ± 2	22 ± 2	29 ± 2	66 ± 1
		4.0	14 ± 2	21 ± 1	28 ± 2	63 ± 3
		4.5	13 ± 1	20 ± 2	27 ± 1	60 ± 2
		5.0	12 ± 3	19 ± 2	26 ± 2	57 ± 1
	98	2.5	16 ± 2	24 ± 1	27 ± 2	67 ± 2
		3.0	15 ± 2	23 ± 2	26 ± 3	65 ± 1
		3.5	14 ± 1	22 ± 3	26 ± 1	62 ± 2
		4.0	13 ± 3	21 ± 1	25 ± 2	59 ± 3
		4.5	12 ± 1	20 ± 2	24 ± 2	56 ± 2
		5.0	11 ± 2	19 ± 3	23 ± 1	53 ± 2

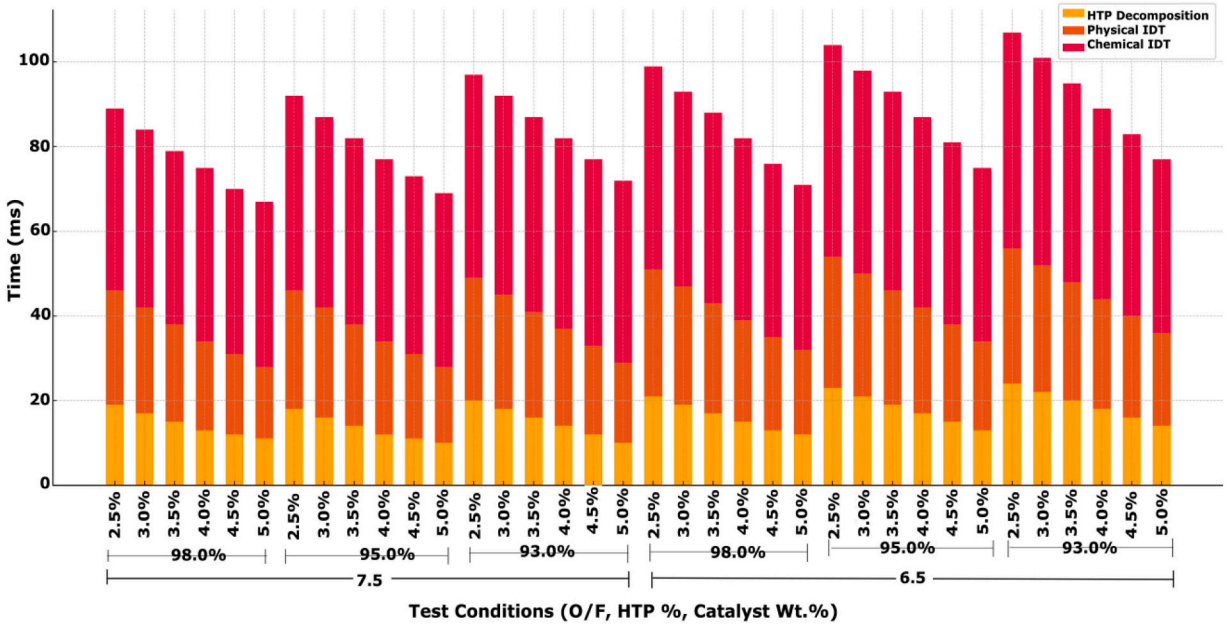

Fig. 6. Contributions of HTP decomposition, physical, and chemical phases to total ignition delay time (ms) across varying HTP concentrations and catalyst loadings for O/F 7.5 and O/F 6.5.

98 % reduced the HTP Decomposition IDT from 11 ms to 9 ms and the Chemical IDT from 31 ms to 20 ms. A higher HTP concentration provides a greater immediate availability of reactive oxygen species upon decomposition, accelerating the subsequent chemical reactions with the fuel.

Comparing O/F 7.5 and O/F 6.5, it is evident that O/F 7.5 generally yields shorter total IDTs. This difference is primarily attributed to shorter HTP Decomposition IDT and Chemical IDT phases at O/F 7.5

compared to O/F 6.5 for similar catalyst and HTP concentrations. For instance, at 98 % HTP and 5.0 % catalyst, the total IDT is 45 ms at O/F 7.5 versus 53 ms at O/F 6.5. This suggests that a more oxidizer-rich environment (O/F 7.5) enhances the efficiency of HTP decomposition and the subsequent fuel-oxidizer chemical reactions, thereby shortening these critical time components.

The analysis of deconvoluted IDTs strongly suggests that the catalyst primarily accelerates both the HTP decomposition phase and the chemical reaction phase. While the catalyst is essential for initiating HTP decomposition, its increasing concentration appears to further speed up this initial step and, more significantly, the rate of the final exothermic chemical reactions between the decomposed HTP products and kerosene. The relatively stable nature of the Physical IDT across varying catalyst loadings and HTP concentrations implies that mass transfer (mixing and vaporization) is either not the rate-limiting step influenced by these parameters, or its acceleration is less pronounced compared to the chemical transformations. This provides deeper mechanistic insight: the catalyst's role is not merely initiating the process but actively accelerating the reactive stages of both propellant breakdown and combustion.

High-speed camera imaging provides direct visual evidence of the distinct phases that constitute the total ignition delay time, as depicted in Fig. 7. This sequence of snapshots captures the critical moments from initial propellant contact to established combustion. Fig. 7(a) captures the moment of initial propellant dispensing at $t = -16$ ms, showing the HTP droplets (circles) just entering the glass bottle before mixing in the doped kerosene. Upon propellant mixing, Fig. 7(b) illustrates the onset of HTP decomposition at $t = 11$ ms, characterized by visible gas evolution (circles) from the oxidizer droplet. This leads to Fig. 7(c) at $t = 29$ ms, representing the physical delay phase, where vaporization and mixing of the propellants become dominant, preparing the reactive interface.

As the mixture reaches critical conditions, Fig. 7(d) at $t = 51$ ms marks the chemical reaction onset, indicated by the first discernible light emission (circle), which signifies the moment of ignition.

This initial ignition kernel then rapidly develops and propagates, as shown in Fig. 7(e) at $t = 60$ ms, depicting a developing ignition kernel, and Fig. 7(f) at $t = 98$ ms, where an establishing flame front forms a stable flame. Fig. 7(g) at $t = 197$ ms captures the stage of full combustion and propagation, indicating peak intensity where propellants are vigorously burning and releasing significant energy. Finally, Fig. 7(h) at $t = 379$ ms illustrates combustion quenching, showing the last visible combustion kernel and signifying the concluding stage of the ignition event. The precise time steps indicated on each frame further quantify the duration of these visually distinct phases, offering a comprehensive understanding of the hypergolic ignition sequence.

3.3.2. *Characteristic temperatures of ignition phases*

Beyond the time durations, the characteristic temperatures reached during different phases provide a thermal profile of the ignition process. Table 3 presents the measured temperatures at the onset of HTP decomposition, during the physical mixing phase, and at the point of significant chemical reaction leading to ignition.

To visualize the trends in these characteristic temperatures, Fig. 8 provides line graphs. The analysis of characteristic temperatures provides insights into the thermal conditions driving each phase. The HTP Decomposition Temperature generally decreases with increasing catalyst loading and higher HTP concentrations. For example, at O/F 7.5 with 98 % HTP, increasing catalyst from 2.5 % to 5.0 % lowers the decomposition temperature from 87 °C to 59 °C. This indicates that a more active catalyst surface or a greater concentration of HTP facilitates decomposition at lower thermal energy inputs, signifying enhanced catalytic efficiency, likely due to improved catalytic surface area or Mn (II)AA redox properties enhancing the decomposition pathway

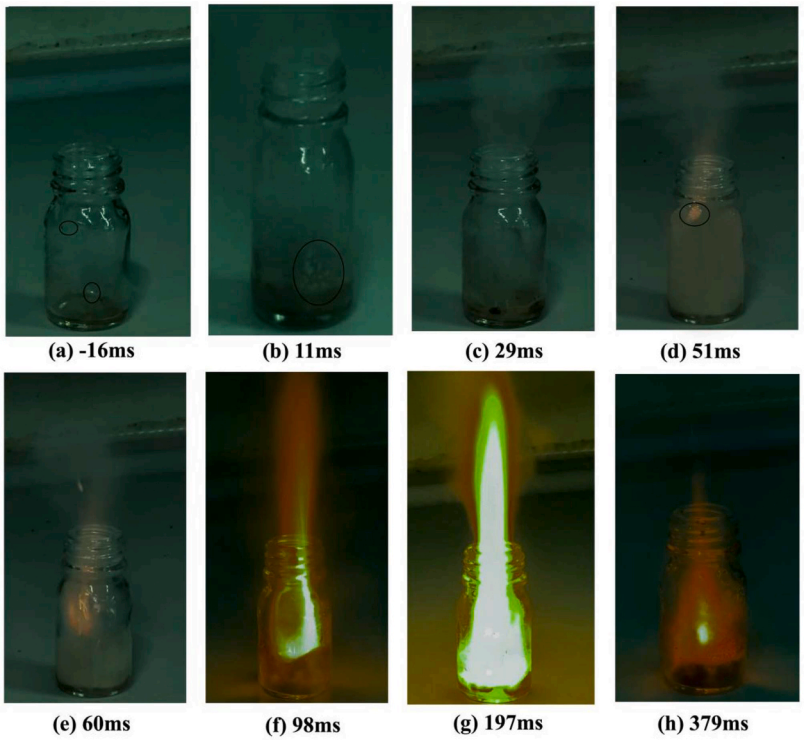

Fig. 7. High-speed camera image sequence illustrating the distinct phases of hypergolic ignition and post-ignition combustion for a representative condition (O/F 7.5, 98 % HTP Conc., 4 % Catalyst, Initial Temperature 50 °C). The sequence captures: (a) Initial Propellant Dispensing ($t = -16$ ms); (b) Onset of HTP Decomposition ($t = 11$ ms), identified by the first objective visual evidence of gas evolution; (c) Physical Delay Phase ($t = 29$ ms), characterized by vapor cloud expansion; (d) Chemical Reaction Onset / First Light ($t = 51$ ms), identified by pixel intensity exceeding the 20 % threshold; (e) Developing Ignition Kernel ($t = 60$ ms); (f) Establishing Flame Front ($t = 98$ ms); (g) Peak Combustion ($t = 197$ ms); and (h) Combustion Quenching ($t = 379$ ms).

Table 3
Characteristic temperatures (°C) for ignition phases.

O/F Ratio	HTP Conc (%)	Catalyst Wt.%	HTP Decomposition Range (°C)	Physical IDT (°C)	Chemical IDT (°C)	Post-Ignition Flame Temp (°C)
7.5	98	2.50	87	144	268	1045
		3.00	79	144	260	1080
		3.50	70	142	253	1115
		4.00	62	142	245	1150
		4.50	61	146	248	1180
		5.00	59	149	251	1210
6.5		2.50	97	142	281	990
		3.00	95	142	276	1016
		3.50	92	143	270	1042
		4.00	91	144	265	1067
		4.50	89	144	260	1093
		5.00	87	144	255	1119
7.5	95	2.50	87	145	262	1005
		3.00	82	147	255	1040
		3.50	76	147	249	1075
		4.00	71	149	242	1110
		4.50	63	146	247	1135
		5.00	55	144	251	1160
6.5		2.50	94	144	275	950
		3.00	89	144	270	977
		3.50	83	144	266	1004
		4.00	78	144	262	1031
		4.50	72	144	258	1058
		5.00	67	144	254	1085
7.5	93	2.50	88	146	267	960
		3.00	83	147	261	995
		3.50	78	147	255	1030
		4.00	73	147	249	1065
		4.50	67	147	252	1090
		5.00	62	147	255	1115
6.5		2.50	94	145	280	910
		3.00	89	145	275	937
		3.50	84	145	270	964
		4.00	79	145	265	991
		4.50	74	146	262	1020
		5.00	69	146	260	1049

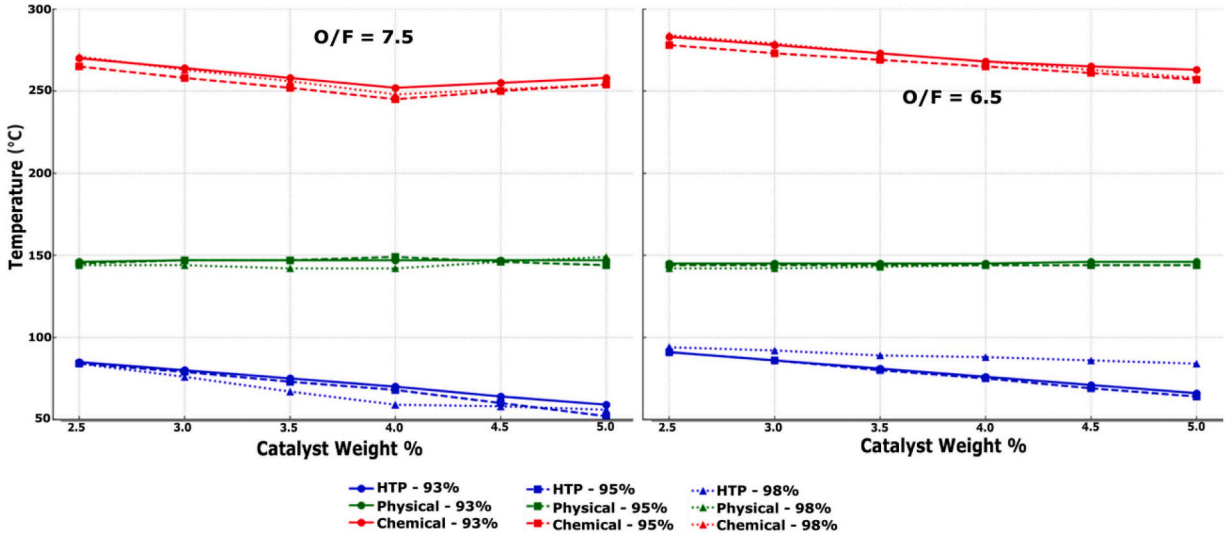

Fig. 8. Characteristic temperatures during HTP decomposition, physical mixing, and chemical reaction phases as a function of catalyst loading, HTP concentration, and O/F ratio. The maximum observed standard deviation was ±8 °C; consequently, error bars are frequently smaller than the data markers. Note: A systematic uncertainty of ±20 °C applies to absolute temperature values due to emissivity variations.

energetics. Higher O/F ratios also tend to show lower decomposition temperatures, suggesting the presence of more oxidizer facilitates the initial breakdown.

The temperature associated with the physical mixing phase remains remarkably consistent across nearly all tested conditions, typically around 142–149 °C. This suggests that the completion of physical mixing and fuel vaporization is primarily dependent on reaching a specific thermal threshold, largely independent of the catalyst concentration or HTP strength. It indicates that once enough heat is generated to vaporize the fuel and allow for adequate mixing, this phase is completed.

The temperature at which the rapid chemical reaction occurs

generally decreases with increasing catalyst loading and higher HTP concentrations. This reduction in the chemical ignition temperature at higher catalyst loadings can be attributed to an increase in the pre-exponential factors in Arrhenius kinetics, which signifies a higher frequency of effective collisions due to a greater number of active catalytic sites. Such an enhancement in reaction kinetics allows the chemical reaction to proceed rapidly at lower thermal energy inputs, consistent with improved catalytic efficiency. For instance, at O/F 7.5 with 98 % HTP, increasing catalyst from 2.5 % to 5.0 % causes the chemical reaction temperature to drop from 268 °C to 251 °C. This implies that a more potent catalyst or a richer oxidizer environment allows the critical exothermic reactions to initiate and propagate at lower temperatures, indicative of improved reaction kinetics and more efficient energy release. Higher O/F ratios also show lower chemical reaction temperatures.

Combining the insights from both the time-resolved IDT phases and their associated characteristic temperatures offers a comprehensive view of the ignition mechanism. The catalyst's primary role is to accelerate the chemical aspects of the ignition process: facilitating HTP decomposition at lower temperatures and completing the main exothermic reactions more quickly and at lower chemical reaction temperatures. While the catalyst significantly shortens the HTP decomposition and chemical reaction durations, the physical mixing phase appears to be a more thermally driven process, requiring a consistent temperature threshold, and its duration is less impacted by changes in catalyst or HTP concentration. This dual analysis reveals that optimizing the catalyst for both initial decomposition and subsequent chemical kinetics is paramount for achieving faster and more robust hypergolic ignition.

3.4. Kinetic analysis and mechanistic insights

Kinetic analysis provides a quantitative framework to understand the underlying mechanisms of hypergolic ignition, yielding critical parameters such as apparent activation energy (E_a) and pre-exponential factor (A). These parameters directly relate to reaction rates, energy barriers, and the catalytic effectiveness of Mn(II)AA. By examining their variation across different catalyst loadings and HTP concentrations for optimal O/F ratios, we can explain observed ignition delay time (IDT) trends and quantitatively assess the catalyst's role, including the phenomenon of diminishing returns.

3.4.1. Physical meaning and interpretation of kinetic parameters

E_a signifies the minimum energy for ignition, while A reflects the frequency of effective molecular encounters. Derived from the Arrhenius Eqs. (4) and (5) ($k \propto 1/IDT$) using IDT data at 20 °C and 50 °C, these parameters are apparent for the overall multi-step hypergolic process, not single elementary reactions. This distinction is important given the multi-step nature of hypergolic ignition involving heterogeneous catalysis and gas-phase reactions.

A key finding is the remarkable consistency of E_a. For all conditions at O/F 6.5, E_a is consistently 10.0 kJ/mol (refer to Supplementary Table S2). Similarly, for O/F 7.5, E_a remains very stable within 10.0 to 10.2 kJ/mol. This low and stable E_a indicates a weak temperature dependence of ignition in the studied range. In contrast, the pre-exponential factor (A) shows significant variability, generally increasing with higher HTP concentrations and catalyst loadings.

The consistently low E_a values (approx. 10.0–10.2 kJ/mol) suggest that, within the 20–50 °C range, the overall ignition process is dominated by steps with low energy barriers. This implies that physical processes (e.g., mass transfer, vaporization, mixing) or surface-controlled catalytic steps may be rate-limiting, as these typically have lower activation energies than purely chemical reactions. The unchanging E_a across conditions underscores this stable temperature sensitivity.

The calculated A values, ranging from 10^2 to 10^3 s^{-1}, are significantly lower than those for typical unimolecular gas-phase reactions (10^{12} to 10^{14} s^{-1}). This difference is characteristic of complex, multi-step processes involving physical phenomena and heterogeneous catalysis, where apparent A factors can be greatly reduced. The monotonic increase in A with higher catalyst loadings and HTP concentrations (Fig. 9) reflects the growing frequency of effective catalytic interactions and reactive encounters, which directly accelerate ignition kinetics. It is important to note that the variability of A is attributed not solely to catalytic surface activity and oxidizer strength but also influenced by factors such as mixing quality and fuel vaporization, which collectively contribute to mechanistic completeness. Thus, while E_a is constant, changes in A are the primary drivers for observed IDT reductions.

Fig. 9 visually represents the trends in the apparent pre-exponential factor (A), which effectively captures the varying kinetic behavior across conditions. The constancy of E_a is primarily conveyed through the textual discussion due to its minimal variation across the studied parameters.

3.5. Sensitivity analysis and limitations of the two-point kinetic method

The kinetic parameters presented above were derived using a two-point Arrhenius approximation (20 °C and 50 °C). It is critical to interpret these values as "apparent" global parameters ($E_{a,\ app}$ and A_{app}) that lump together the effects of physical processes (atomization, vaporization, mixing) and complex multi-step chemical reactions. While a multi-point temperature sweep would yield higher fidelity, the two-point method serves here as a robust screening tool to identify relative catalytic trends across the extensive experimental matrix.

A sensitivity analysis was conducted to quantify the impact of measurement noise on the derived activation energy. Propagating the experimental standard deviation of the ignition delay time ($\sigma_{IDT} \approx 1.7$ ms) and a temperature uncertainty of ±1 K into the Arrhenius equation reveals an uncertainty in E_a of approximately ±1.2 kJ/mol.

$$\delta E_a \approx R \cdot \left|\frac{T_1 T_2}{T_2 - T_1}\right| \cdot \sqrt{\left(\frac{\sigma_{IDT1}}{IDT_1}\right)^2 + \left(\frac{\sigma_{IDT2}}{IDT_2}\right)^2} \quad (6)$$

Even accounting for this uncertainty, the calculated E_a values consistently fall within the narrow range of 10.0–11.5 kJ/mol. This low magnitude, statistically distinct from the higher activation energies typical of pure hydrocarbon oxidation, confirms the dominant role of the catalyst in lowering the energy barrier and underscores the stability of the kinetic conclusion despite the two-point limitation.

3.5.1. Role of Mn(II)AA as an effective catalyst and diminishing returns

The derived kinetic parameters quantitatively confirm Mn(II)AA's effectiveness as a hypergolic catalyst. Although E_a remains consistent, the significant increase in A with increasing catalyst loading and HTP concentration (Fig. 9) clearly shows the catalyst's role in accelerating ignition by enhancing effective reactive events. The catalysis is likely driven by Mn(II)AA-facilitated redox decomposition of H_2O_2, forming reactive radicals (e.g., OH*, O_2^{*-}) that initiate exothermic oxidation of kerosene vapors.

Furthermore, the data robustly illustrates the concept of diminishing returns. As observed in Fig. 7, the rate of increase in the pre-exponential factor (A) notably slows down as catalyst loading rises from 5 % to 7.5 % and further to 10 %. This diminishing return is quantitatively evident; for example, for 98 % HTP, the average slope of ln(A) with respect to catalyst wt. % dramatically decreases from approximately 0.124 for the 2.5–5.0 % catalyst range to about 0.014 for the 5.0–7.5 % range. This represents an approximate 89 % reduction in the rate of kinetic acceleration per unit increase in catalyst loading. Further, the slope nearly plateaus at approximately 0.013 for the 7.5–10.0 % range, indicating minimal additional benefit from increasing catalyst concentration beyond 7.5 %. This flattening of the A vs. catalyst loading curve suggests a saturation regime, where beyond 5 wt %, further increases offer

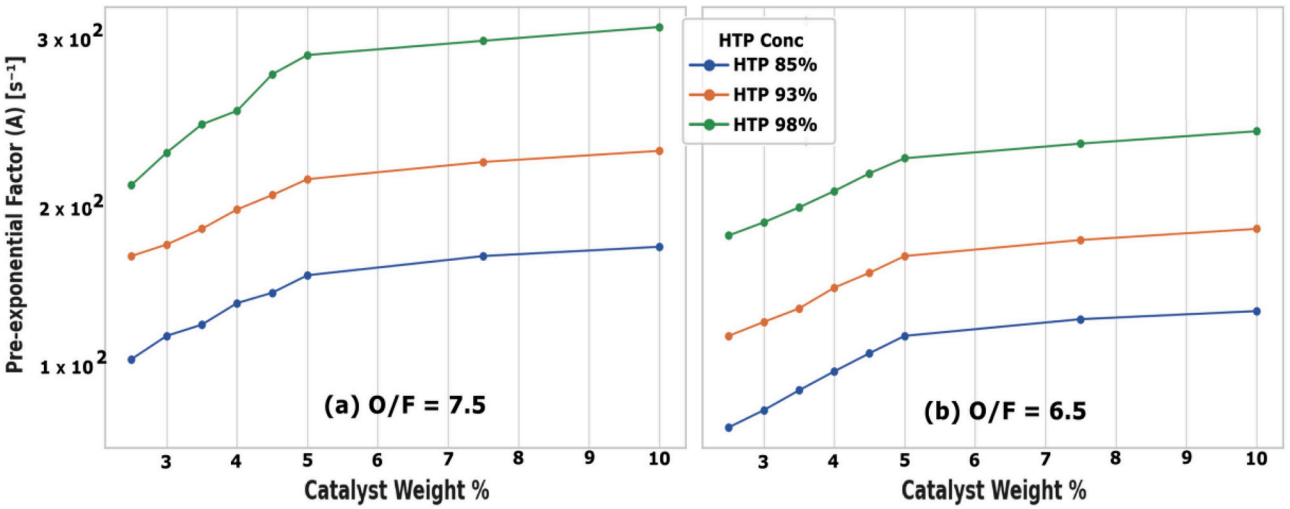

Fig. 9. Apparent pre-exponential factor (A) as a function of catalyst loading and HTP concentration for (a) O/F 7.5 and (b) O/F 6.5, demonstrating the kinetic effects on hypergolic ignition and illustrating the diminishing returns beyond 5 % catalyst weight.

diminishing kinetic benefits due to the emergence of non-chemical rate limitations such as mass transport or intrinsic decomposition rates. These physical steps are less responsive to further increases in chemical reaction rates achieved by higher catalyst concentrations, leading to a saturation effect in IDT performance.

3.6. *Post-ignition flame temperatures – energy release and performance*

Post-ignition flame temperature is a critical indicator of combustion efficiency and the extent of energy release within hypergolic propulsion systems. These temperatures directly reflect the conversion of the propellants' chemical energy into thermal energy, thereby influencing crucial performance metrics such as specific impulse. The measured peak flame temperatures are presented in Fig. 10, which illustrates their relationship with catalyst weight percentage for different O/F ratios and HTP concentrations.

As depicted in Fig. 10, post-ignition flame temperatures consistently increase with higher catalyst loadings across all tested HTP concentrations and O/F ratios. For instance, at O/F 7.5 with 98 % HTP, increasing catalyst from 2.5 % to 5.0 % led to a notable rise in flame temperature from 1045 °C to 1210 °C. Similarly, higher HTP concentrations consistently yield elevated flame temperatures; for a given catalyst loading (e.g., 5.0 %), switching from 93 % HTP to 98 % HTP at O/F 7.5 resulted in flame temperature increases from 1115 °C to 1210 °C. Furthermore, O/F 7.5 generally produces higher post-ignition flame temperatures than O/F 6.5 across comparable conditions, indicating improved oxygen

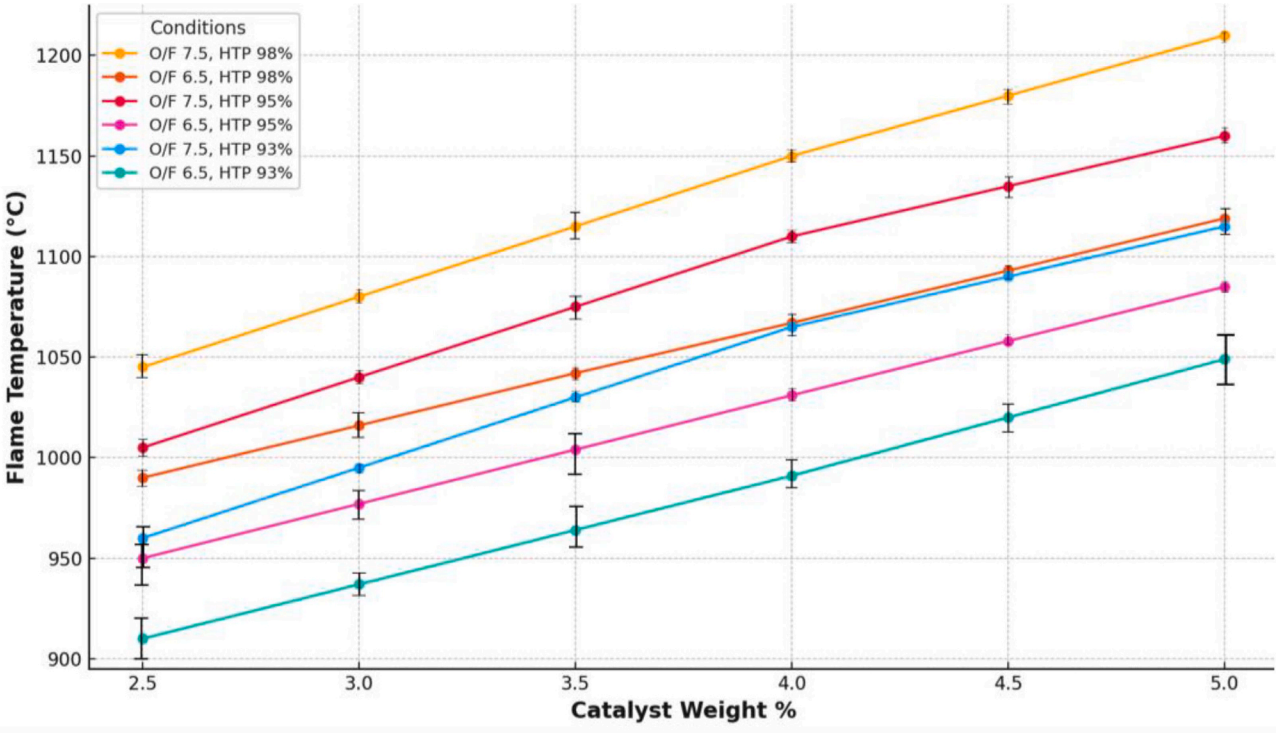

Fig. 10. Variation in post-ignition flame temperatures as a function of catalyst weight percentage for different O/F ratios and HTP concentrations. Error bars represent the standard deviation ($n = 5$); where not visible, error bars fall within the area of the data point.

availability at the higher O/F ratio contributes to more exothermic reactions.

The observed flame temperatures provide direct insights into the energy release and combustion efficiency of the hypergolic reaction. Higher post-ignition flame temperatures signify a more complete and efficient combustion process, translating to a greater conversion of the propellants' chemical energy into thermal energy. This indicates that the Mn(II)AA catalyst not only facilitates rapid ignition but also promotes a more thorough reaction once initiated. Strong correlations exist between flame temperatures and other key ignition parameters: as catalyst loading increases, both the apparent pre-exponential factor (A) (Fig. 9) and post-ignition flame temperatures increase, while IDTs decrease. This signifies that higher catalyst concentrations contribute to both faster ignition and more complete combustion, thereby optimizing energy release. Similarly, elevated HTP concentrations correlate with shorter IDTs and significantly higher flame temperatures, primarily due to the greater availability of oxidizer for reaction. Moreover, an inverse relationship is observed between IDT and flame temperature, where shorter IDTs are often associated with higher flame temperatures, indicating that rapid and complete mixing and reaction lead to more efficient energy release.

From a propulsion system perspective, achieving higher post-ignition flame temperatures is highly desirable as it directly correlates with enhanced performance. Elevated flame temperatures translate to higher specific impulse (I_{sp}) due to a greater thermal energy content of the exhaust gases, leading to increased thrust and contributing to enhanced stability and efficiency of the propulsion system. Therefore, Mn(II)AA's ability to not only significantly reduce ignition delay but also to promote higher post-ignition flame temperatures underscores its potential as an effective catalyst for improving overall performance and efficiency in HTP/kerosene-based propulsion systems. While kinetic analysis in Section 3.4 demonstrated diminishing returns for IDT reduction beyond certain catalyst loadings, the flame temperature data, available up to 5 % catalyst weight, consistently shows continued increases with catalyst loading, suggesting that the benefits in energy release persist within this measured range.

3.7. Comparison with alternative catalysts and baseline performance

To contextualize the performance of Mn(II)AA, it is critical to evaluate it against both the baseline non-catalyzed system and other common metal-organic catalysts. Experiments conducted with neat kerosene (0 wt % catalyst) and HTP at both ambient (20 °C) and elevated (50 °C) conditions confirmed that the fuel and oxidizer combination is non-hypergolic. In the absence of the catalyst, no ignition was observed even after extended contact times (>5 s), verifying that the Mn(II)AA additive is the sole driver of the hypergolic initiation in this system. Consequently, the 0.5 wt % loading represents the practical lower limit for reliable hypergolicity in this system.

Fe(III) and Cu(II) acetylacetonates are frequently cited in literature as effective catalysts for HTP systems. Previous studies typically report IDTs for these catalysts in the range of 20–100 ms, depending on the specific solvent and fuel blend [22,24]. The Mn(II)AA system investigated here achieves ignition delays as low as 40 ms, demonstrating competitiveness with these established catalysts.

However, a distinct advantage of the Mn(II)AA catalyst used in this study is its high direct solubility in kerosene. While Fe(III) acetylacetonates often exhibit limited solubility in pure hydrocarbons, frequently requiring co-solvents (such as ethanol or tetraglyme) to achieve sufficient loading, Mn(II)AA was dissolved directly into the fuel up to 10 wt % with excellent stability. This simplifies the propellant formulation and increases the energy density by eliminating non-energetic solvents.

Furthermore, the peak flame temperatures observed in this study (exceeding 1200 °C) indicate robust combustion efficiency. These values are consistent with high-performance hypergolic interactions, confirming that Mn(II)AA not only initiates the reaction rapidly but also facilitates substantial energy release.

3.8. Effect of chamber pressure on applicability

It is crucial to contextualize the measured IDT values (ranging from approximately 59 to 150 ms) within the experimental conditions, as all tests were conducted in an open-air, ambient-pressure setup. Published literature consistently reports significantly reduced IDTs for hypergolic systems when tested under pressurized conditions typical of actual propulsion environments. In particular, ignition delay times measured under ambient conditions typically decrease by about 20–30 % when tests are conducted under elevated pressures [31]. Certain literature reported approximately a 30 % reduction in IDT when transitioning from ambient to pressurized conditions (~1 bar), indicating a substantial potential for further improvement in realistic rocket engine conditions [32,33]. Therefore, the ambient results presented here should be viewed as a conservative upper bound. Future work must explicitly focus on high-pressure validation to quantify these scaling effects and confirm the suitability of Mn(II)AA-doped propellants for regenerative cooling and combustion stability in flight-ready engines.

4. Conclusions

This study provides a comprehensive kinetic and mechanistic evaluation of Mn(II)AA-catalyzed hypergolic ignition in HTP–kerosene systems. Beyond the fundamental kinetic data, the results offer actionable insights for the design and optimization of green bipropellant propulsion systems:

- **Operational Envelope for Reliability:** Reliable hypergolic ignition at ambient pressure is achieved with catalyst loadings 2.5 wt % and HTP concentrations 93 %. Designers targeting robust start-up sequences should prioritize these thresholds to avoid hard starts or ignition failures.
- **Optimal Catalyst Loading:** While higher catalyst concentrations accelerate kinetics, a clear regime of diminishing returns is identified beyond 5 wt % loading. Consequently, an operational loading of 4.5–5.0 wt % is recommended as the engineering optimum, balancing rapid ignition (approx. 45–55 ms at ambient) with propellant cost and solubility limits.
- **Thermal Management and Warm-Starts:** Preheating the fuel to 50 °C yielded a consistent ~33 % reduction in ignition delay time across all mixtures. This suggests that propulsion systems employing regenerative cooling loops or tank heaters to implement "warm-start" protocols can significantly minimize ignition lag and enhance combustion stability without altering the chemical formulation.
- **Injector Design Implications:** Phase deconvolution revealed that the catalyst primarily accelerates the chemical reaction phase, while the physical mixing delay remains relatively constant (~20 ms) regardless of catalytic activity. Therefore, to further reduce total ignition delay, future injector designs should focus on mechanical atomization improvements (e.g., higher pressure drops, impinging jet elements) to shorten the physical mixing timescale, which is now the limiting factor.
- **Future High-Pressure Validation:** Finally, while ambient pressure testing established the baseline efficacy of the Mn(II)AA catalyst, future campaigns must prioritize high-pressure validation. Confirming the expected inverse-pressure scaling ($IDT \propto P^{-n}$) is the critical next step to qualifying this green propellant combination for flight-ready regenerative engines.

These insights establish Mn(II)AA as a viable catalyst for green hypergolic propulsion and offer a framework for transitioning to non-toxic, high-performance ignition systems.

CRediT authorship contribution statement

Prakhar Jindal: Writing – original draft, Visualization, Validation, Resources, Methodology, Investigation, Funding acquisition, Formal analysis, Data curation, Conceptualization. **Jyoti Botchu:** Writing – review & editing, Project administration, Funding acquisition, Formal analysis.

Declaration of competing interest

The authors declare the following financial interests/personal relationships which may be considered as potential competing interests: Prakhar Jindal reports financial support was provided by European Commission Marie Sklodowska-Curie Actions. If there are other authors, they declare that they have no known competing financial interests or personal relationships that could have appeared to influence the work reported in this paper.

Acknowledgements

This material is based upon the work supported by Horizon Europe's research and innovation programme under the Marie Sklodowska-Curie grant agreement No. 101107214. The authors acknowledge the extensive support from the Space System Engineering section of the Faculty of Aerospace Engineering, Delft University of Technology, Netherlands.

Supplementary materials

Supplementary material associated with this article can be found, in the online version, at doi:10.1016/j.rineng.2025.108699.

Data availability

Data will be made available on request.

References

[1] D. Musielak, Liquid propellant rocket engines, (2025) 133–195. 10.1007/978-3-031-86141-3_4.
[2] P. Caisso, A. Souchier, C. Rothmund, P. Alliot, C. Bonhomme, W. Zinner, R. Parsley, T. Neill, S. Forde, R. Starke, W. Wang, M. Takahashi, M. Atsumi, D. Valentian, A liquid propulsion panorama, Acta Astronaut. 65 (2009) 1723–1737, https://doi.org/10.1016/J.ACTAASTRO.2009.04.020.
[3] P. Siddharth, D.K. Bajaj, S. Joshi, Green propellant — the future of space propulsion systems, Adv. Aerosp. Technol. (2024) 73–87, https://doi.org/10.1201/9788770046299-4.
[4] T.D. Kubal, Characterization of Rheological and Ignition Properties of Hypergolic Propellants, Purdue University, 2010. https://docs.lib.purdue.edu/dissertations/AAI1489556/. accessed June 22, 2025.
[5] D.D. Evans, T.W. Price, The status of monopropellant hydrazine technology, 1968.
[6] G.A. Lewandowski, Control of vapor emissions from hydrazine-based fuels. https://apps.dtic.mil/sti/citations/ADA086687, 1980 accessed June 22, 2025.
[7] Y. Ju, C. Song, B.J. Lee, Guidelines for the safe handling of hypergolic propellants in development of space propulsion systems, J. Propuls. Energy 4 (2024) (2024) 42–57, https://doi.org/10.6108/JPNE.2024.4.1.042, 1 4.
[8] N.R.C. (US) C. on A.E.G. Levels, Hydrazine acute exposure guideline levels. https://www.ncbi.nlm.nih.gov/books/NBK220003/, 2010 accessed June 22, 2025.
[9] H.V.N. Nguyen, J.A. Chenoweth, V.S. Bebarta, T.E. Albertson, C.D. Nowadly, The toxicity, pathophysiology, and treatment of acute hydrazine propellant exposure: a systematic review, Mil. Med. 186 (2021) e319–e326, https://doi.org/10.1093/MILMED/USAA429.
[10] S. Park, H. Kang, Y. Park, J. Lee, A review of the technical development on green hypergolic propellant, J. Korean Soc. Propuls. Eng. 24 (2020) 79–88, https://doi.org/10.6108/KSPE.2020.24.4.079.
[11] F.A.S. Mota, L. Fei, M. Liu, J. Jiang, C. Tang, Novel hypergolic green fuels with hydrogen peroxide for propulsion systems, J. Propuls. Power 40 (2024) 207–219, https://doi.org/10.2514/1.B39224;PAGE:STRING:ARTICLE/CHAPTER.
[12] S.M. Davis, N. Yilmaz, Advances in hypergolic propellants: ignition, hydrazine, and hydrogen peroxide research, Adv. Aerosp. Eng. 2014 (n.d.) 729313. 10.1155/2014/729313.
[13] W. Florczuk, G. Rarata, Performance evaluation of the hypergolic green propellants based on the HTP for a future next-generation space crafts, in: 53rd AIAA/SAE/ASEE Joint Propulsion Conference, 2017, p. 2017, https://doi.org/10.2514/6.2017-4849. SUBPAGE:STRING:ABSTRACT;CSUBTYPE:STRING:CONFERENCE.
[14] B.M. Melof, M.C. Grubelich, Investigation of hypergolic fuels with hydrogen peroxide, in: 37th Joint Propulsion Conference and Exhibit, 2001, https://doi.org/10.2514/6.2001-3837. WEBSITE:WEBSITE:AIAA-SITE;REQUESTEDJOURNAL:JOURNAL:6.JPC;WGROUP:STRING:AIAA.
[15] L. Blondel-Canepari, A. Sarritzu, A. Pasini, A holistic approach for efficient greener in-space propulsion, Acta Astronaut. 223 (2024) 435–447, https://doi.org/10.1016/J.ACTAASTRO.2024.07.023.
[16] D. Andrews, H. Sunley, The Gamma Rocket Engines for black knight, J. Br. Interplanet. Soc. 43 (1990) 301–310.
[17] D. Millard, A review of UK space activity and historiography, 1957–2007, Acta Astronaut. 66 (2010) 1291–1295, https://doi.org/10.1016/J.ACTAASTRO.2009.10.007.
[18] G. Rarata, P. Surmacz, Developing and testing new composite catalytic bed for decomposition of 98% HTP, in: 65th International Astronautical Congress, Toronto, 2014. https://www.researchgate.net/publication/283216165_DEVELOPING_AND_TESTING_NEW_COMPOSITE_CATALYTIC_BED_FOR_DECOMPOSITION_OF_98_HTP.
[19] S. Carlotti, F. Maggi, Novel strategies for HTP decomposition: characterization of 3D-printed catalysts, AIAA SciTech Forum Expo. 2024 (2024), https://doi.org/10.2514/6.2024-1790. GROUPTOPIC:TOPIC:LONG_TOC_PUBS>LT_ENABLED;CTYPE:STRING:BOOK.
[20] A.A. Kozlov, I.N. Borovik, A.A. Ermashkevich, V.P. Tashev, S.L. Guseinov, V. A. Kosykh, Self-ignition of fuel consisting of hydrogen peroxide, kerosene, and pyrophoric additives, Russ. Eng. Res. 40 (2020) 208–213, https://doi.org/10.3103/S1068798X20030107/FIGURES/5.
[21] S.L. Guseinov, S.G. Fedorov, V.A. Kosykh, P.A. Storozhenko, Hydrogen peroxide decomposition catalysts used in rocket engines, Russ. J. Appl. Chem. 93 (2020) 467–487, https://doi.org/10.1134/S1070427220040011.
[22] S.L. Guseinov, S.G. Fedorov, V.A. Kosykh, P.A. Storozhenko, Hypergolic propellants based on hydrogen peroxide and organic compounds: historical aspect and current state, Russ. Chem. Bull. 67 (2018) 1943–1954, https://doi.org/10.1007/S11172-018-2314-1/METRICS.
[23] T.L. Pourpoint, W.E. Anderson, Hypergolic reaction mechanisms of catalytically promoted fuels with rocket grade hydrogen peroxide, Combust. Sci. Technol. 179 (2007) 2107–2133, https://doi.org/10.1080/00102200701386149.
[24] Y. Cong, T. Zhang, T. Li, J. Sun, X. Wang, L. Ma, D. Liang, L. Lin, Propulsive performance of a hypergolic H2O2/Kerosene bipropellant, J. Propuls. Power 20 (2004) 83–86, https://doi.org/10.2514/1.9189. WEBSITE:WEBSITE:AIAA-SITE;WGROUP:STRING:AIAA.
[25] S.L. Guseinov, S.G. Fedorov, V.A. Kosykh, V.A. Vaulin, Hypergolic propellants based on high-test hydrogen peroxide and organic compounds, Russ. J. Appl. Chem. 96 (2023) 873–888, https://doi.org/10.1134/S1070427223100014/TABLES/2.
[26] G.B. Shul'Pin, Y.N. Kozlov, L.S. Shul'Pina, T.V. Strelkova, D. Mandelli, Oxidation of reactive alcohols with hydrogen peroxide catalyzed by manganese complexes, Catal. Lett. 138 (2010) 193–204, https://doi.org/10.1007/S10562-010-0398-9/METRICS.
[27] KR20190010207A - Auto-ignition gel propellant - Google Patents. https://patents.google.com/patent/KR20190010207A/en?q=(Auto-ignition+gel+propellants)&oq=Auto-ignition+gel+propellants#citedBy, 2019 accessed June 29, 2025.
[28] KR101441020B1 - Gelled fuel and gelled oxidizer for gel propellant - Google Patents. https://patents.google.com/patent/KR101441020B1/ko?q=(ECB694ECA784ECA09CEC8B9CEC8AA4ED859CEC9D84EC9C84ED959CECA0A4ED9994EB909CEC97B0EBA38CEBB08FEC82B0ED9994ECA09C+.)&oq=ECB694ECA784ECA09C+EC8B9CEC8AA4ED859CEC9D84+EC9C84ED959C+ECA0A4ED9994EB909C+EC97B0EBA38C+EBB08F+EC82B0ED9994ECA09C.&page=1, 2014 accessed June 29, 2025.
[29] US20220324710A1 - Process and apparatus for concentrating hydrogen peroxide to 98 wt.% or more - Google Patents, (n.d.). https://patents.google.com/patent/US20220324710A1/en?oq=US17775065:+Process+and+apparatus+for+concentrating+hydrogen+peroxide+to+98%25+wt%25+or+more. (accessed June 29, 2025).
[30] NL2024229B1 - Economical and Simplified In-Situ Concentration to 98%+ Hydrogen Peroxide - Google Patents, (n.d.). https://patents.google.com/patent/NL2024229B1/en?oq=NL2024229B1:+Simplified+in-situ+hydrogen+peroxide+concentration+technology (accessed June 29, 2025).
[31] B.V.S. Jyoti, M.S. Naseem, S.W. Baek, Hypergolicity and ignition delay study of pure and energized ethanol gel fuel with hydrogen peroxide, Combust. Flame 176 (2017) 318–325, https://doi.org/10.1016/J.COMBUSTFLAME.2016.11.018.
[32] Ł.J. Kapusta, Ł. Boruc, J. Kindracki, Pressure and temperature effect on hypergolic ignition delay of triglyme-based fuel with hydrogen peroxide, Fuel 287 (2021) 119370, https://doi.org/10.1016/J.FUEL.2020.119370.
[33] D.A. Castaneda, B. Natan, Hypergolic ignition of hydrogen peroxide with various solid fuels, Fuel 316 (2022) 123432, https://doi.org/10.1016/J.FUEL.2022.123432.